ERT and GPR as Potential Geophysical Tools for Detecting Clandestine Buried Forensic Evidence

Bachelor Thesis BSc *Applied Earth Sciences*

Claire Mulder
Student Number: 4435729

In cooperation with : Frederikke Hansen - 4531369
Supervisors TU Delft : Evert Slob, Guy Drijkoningen
Supervisors NFI : Coen Nienaber

Abstract

Forensic investigations focused on determining clandestine buried weapons, narcotics or even homicide evidence, can be expensive, inefficient and depend greatly on prior information and the tools available. Geophysical tools have potential to improve these investigations, on the ground that they can detect shallow buried objects in a non-invasive way. This report studies the use of electrical resistivity tomography (ERT) in combination with ground penetrating radar (GPR) to detect buried objects at two different sites, both with conditions found here in The Netherlands. The first is a test site at the Technical University of Delft, The Netherlands. Here, two plastic barrels are buried, one is empty and the other is filled with metal rods. The second site is at the ARISTA Facility in Amsterdam, The Netherlands. Here, human cadavers are buried for forensic research. The ERT was used in two ways, the first was to produce 2 dimensional (2D) surveys, which were combined to create a 3 dimensional (3D) model. The second method made measurements that created a 3D model directly. For each the dipole-dipole array was used. At the TU Delft site the results for the 2D method showed clear resistivity anomalies at the locations of the barrels. These anomalies corresponded to clear reflections in the GPR radargrams. The results at the ARISTA facility are inconclusive due to damage in the instrument used. The grid designs made for both ERT methods could however be used in a continuation of this study, and future research should be done within this topic to improve forensic investigations.

Acknowledgements

The data acquisition was done together with Frederikke Hansen who has written a thesis focusing on the use of GPR in forensic investigations. We would like to thank Evert Slob and Guy Drijkoningen for supervising us during this project. They provided insightful information and gave helpful feedback to build on. We would also like to thank Coen Nienaber, our supervisor from the Netherlands Forensic Institute, who helped during the acquisition in Amsterdam and organized access to the facility, and transportation for all the equipment. Lastly, we want to thank Juan Chavez Olalla for making time to help us get familiarized with all the equipment, and spending hours to help us process the data and answering all our questions. We have both learnt so much during this short amount of time, which will enrich our future studies.

Contents

1 Introduction

1.1 General Problem

Since 2006 a total of 41 clandestine graves have been found in The Netherlands as a result of a homicide investigations (W.J.M. Groen, June 2019). Following a murder case where the body is missing, a team of specialized people from the police and the Netherlands Forensic Institute (NFI) go on a search for the missing body. This can take up to a few weeks, depending on the available information leading to the body location. Searches like these are vital for the conviction of a murderer, yet they can be inefficient and costly, and time is considered valuable in this context. The use of technology is therefore under development, more specifically geophysical technologies as tools for forensic investigations. Various geophysical methods have potential within forensics, on the grounds that they can detect shallow buried objects which are in this case forensic evidence such as weapons, and human bodies. Their non-invasive nature are beneficial, as it will not interfere with any murder evidence. This research project will focus on using electrical resistivity tomography (ERT) to detect buried plastic barrels used to simulate buried narcotics or weapons at the Technical University of Delft, and also cadavers at a research facility in Amsterdam, The Netherlands. To analyze ERT as a forensic tool, models of the buried objects, along with models of the ground with and without a body will be made and compared. For verification, images made with a ground penetrating radar (GPR) will be used.

The goal of this report is to describe the methods, sites and results of this research, and to answer the research questions stated below. The issues encountered during fieldwork and data processing are also explained, and recommendations are given for further research. A short overview of human taphonomy is also given, to form an idea of the state of the body that was investigated.

1.2 Literature Research

ERT has been a widely used tool for detecting buried objects that are close to the surface. For example, detecting tombs from hundreds of years ago with ERT, which proved to be successful referring to a study done in Greece [10]. Or detecting the boundaries of a mass burial from the Spanish war through a combination of 2D and 3D surveying [9]. The applications of ERT are still being established, and using it to detect clandestine graves is a relatively new concept, especially in environments found in The Netherlands.

To achieve a more integrated approach, GPR surveys are used. In an article by Geoffrey Jones [7], it was stated that the use of GPR is very common for the investigation of old cemeteries, which is an application that is related to the focus of this report. The quality of GPR surveys is however very dependent on site conditions, as it highly favours soils that are low in conductivity such as sand. The research facility in Amsterdam is made up of sandy soils, which is why the GPR is an appropriate method to use as verification.

The buried body at the facility in Amsterdam was buried around the end of March, 2018. This means around the body had been buried for about 14 months at the time the GPR and ERT surveys were done. A human body goes through 4 stages of decay once it has been defined dead [12]. The first stage is known as 'autolysis', where the deprivation of oxygen leads to a build up of carbon dioxide and waste, and the cells break open, spilling out fluids. Next, the body begins to bloat due to the gases produced by the bacteria in the body. The following step is the breaking down of soft tissue by micro-organisms. Concomitantly larger carnivorous insects aid the decomposition process, and this is referred to as active decay. Once all edible tissue has been consumed, and all fluids have left the body, the process enters the final stage which results in skeletonization [12].

The overall time scale of this process varies greatly with temperature. Higher average temperatures will result in faster decay. A rough estimate for time till skeletonization can be made using the following formula: $t = \frac{1285}{T}$ where t = time in days and T = average temperature in °C [12]. With an average temperature of about 14 °C [11], it can be estimated that it took around 90 days until the observed body was skeletonized. Therefore bone and dry skin remains can be expected.

This description of human decay is in it's general form, but can vary in different post-mortem environ-

ments. This thesis is focused on clandestine graves, where the body is fully buried, wearing no clothes. Luckily, because the two other bodies at this facility are used to study the impact of insects on human decomposition, they have been taken out of the ground and put back in. Subsequentially, the above estimation of the state of the body is quite accurate, and this can be taken into further consideration when analyzing the data.

1.3 Research Question

The overall research question is: How does ERT behave as a forensic tool to detect clandestine buried forensic evidence? To investigate this question, the following sub-question has been formulated:

- Can the location of buried plastic barrels be determined using 3D resistivity models obtained from 2D surveys?

This subquestion will be answered using the ERT models and comparing them with radargrams made with the GPR.

A second sub-question was formulated to describe the behaviour of ERT as a tool to detect clandestine graves: 'Which differences can ERT detect between a burial site and a non-burial site?'. This question should be taken into consideration when a continuation of this research is done.

2 Sites

Two sites were used to perform the ERT and GPR data acquisition. The first site at the TU Delft campus was used to learn how each method worked and how to work efficiently. Together with Juan Chavez Olalla, a PhD Student at the TU Delft, we created a set-up and plan on how to work with the equipment properly and safely. The second site is the ARISTA facility. At this facility, the methods used at the campus were applied after a few adjustments. This chapter will show an overview of the two sites, their location and a description of each. It will also describe the location of the grids for both the ERT and GPR.

2.1 TU Delft test site

The site at the TU Delft is a 4.5 $\times$ 4.5 meter plot, with 3 buried items. One small empty barrel, one barrel with steel rods, and one spot where the ground was dug up and put back in. This location was used as the focus of two bachelor's theses last year [6],[13]. The purpose of this site was to detect differences in the imaging of these buried objects in wet and dry conditions, and in the long term look at compaction effects. The exact location of this site was determined using pictures from last year, and the location of our test grid is shown below in Figure 1. This was found using measuring tapes and by using buildings nearby as reference. A GPS did not work here due to the amount of buildings and trees present. Figure 3 shows the grid from last year, but with slightly different coordinates than those in Figure 2. Assuming the grids do align, then based on the coordinate grid in Figure 2, the following coordinates define the location of the 3 objects:

	Coordinate corresponding to grid in Figure 2
Empty barrel	(4.75 , 0.5)
Barrel filled with steel rods	(3.25 , 1.5)
Back-filled pit	(1.25 , 4)

Table 1: Coordinates of buried barrels and back-filled pit at TU Delft site

Both the ERT and GPR were used here, but only the 2D dipole-dipole method was used as the 3D out of plane method was not yet designed at this stage. These methods are described in Sections 3.5.1 and 3.5.2. The original 0.5 meter electrode spacing shown in Figure 8 was used. Figure 2 shows the exact grids used for both the ERT and GPR. The boundaries of the GPR grid correspond to the center of the first GPR line. The GPR grid also corresponds to the grid shown in Figure 1. The ERT grid is slightly offset, by 20 cm. During acquisition, we started by looking at pictures and grids from last years reports, and based on this we took a few GPR samples. We located the position of what we assumed to be the empty barrel. The ERT grid was then set up to surely include this empty barrel location, and we tried to position the grid as close to last years grid as possible, to also include the filled barrel and the empty pit. After the ERT acquisition was complete, we kept the boundaries and used these for the GPR. The first GPR line was then made by aligning the cart to the ERT boundary. Because the GPR cart is 40 cm wide, this means that the center line was at 20cm away from the ERT grid boundary. This explains the 20 cm offset in both directions.

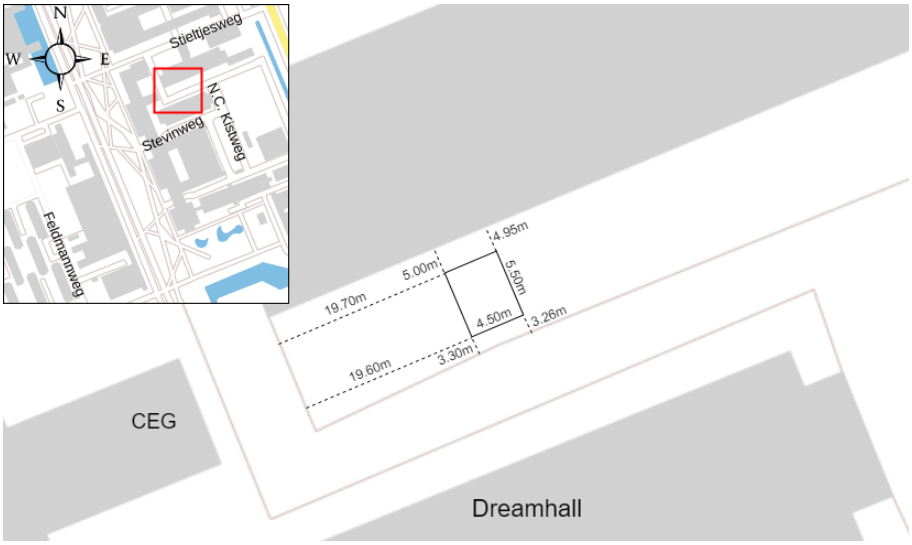

Figure 1: Location of TU Delft test site

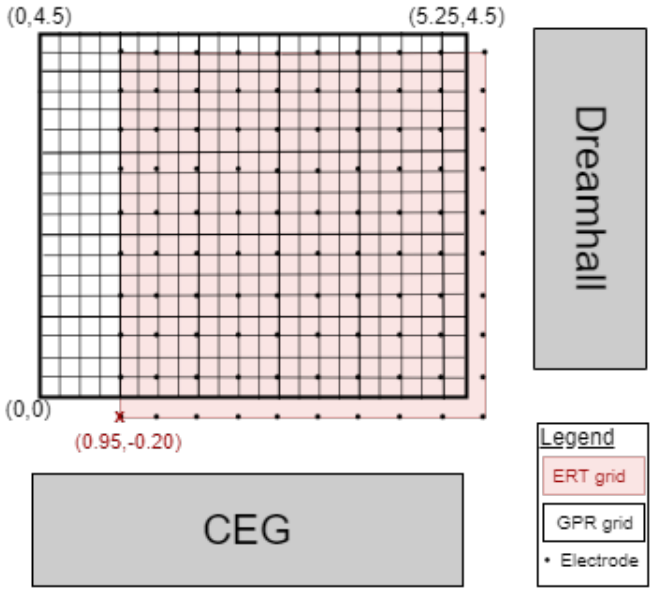

Figure 2: TU Delft GPR and ERT Grid

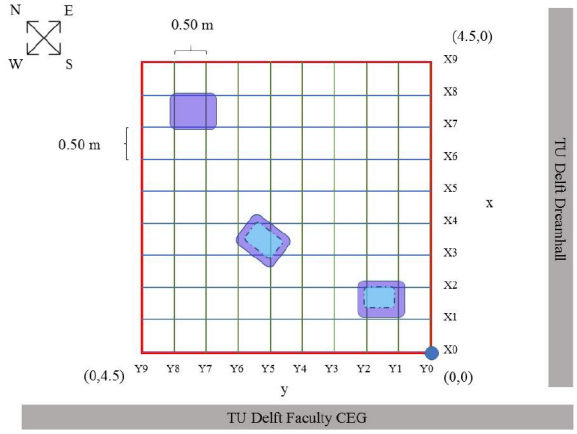

Figure 3: Buried barrel locations at TU Delft; bottom right barrel is empty, middle is filled with metal rods, top left is an excavated and filled pit [6].

2.2 ARISTA Facility

ARISTA stands for Amsterdam Research Initiative for Sub-surface Taphonomy and Anthropology. This facility was opened in 2018 to research the decay of human bodies in conditions found here in The Netherlands. In total 10 of these facilities exist in the world, with eight in the USA, one in Australia and the last being the facility in the Netherlands [3]. The exact location is shown in Figure 4. The research done at these facilities has varying applications. One of these being to observe the stages in which a body decays , but also for forensic sciences and how to detect a body using non invasive methods. Currently there are three bodies residing at the ARISTA facility. Two bodies are used to study entomology (how insects affect the decay of a body), and the third is used for non invasive, remote sensing research. This body will be used as focus of this study, and it is buried in a pit that is 0.6 meters deep. This research will aid in criminal investigations, more specifically in detecting a clandestine buried body. The soil is predominantly made up of sand, and there are many plants and roots in the ground.

For this project we were allowed two days access to the facility. This gave enough time to perform all surveys on a filled grave on one day, and an empty pit on the other. In Figure 4, the B is the location of the filled grave, and P is the location of the empty pit. Here, the GPR was used, along with both the ERT methods explained in Sections 3.5.1 and 3.5.2. Figures 5 and 6 show the grids used for both methods, and their dimensions. Due to spatial constraints, the electrode spacing was shortened to 0.30 meters. This does

not however change the electrode numbering or the array inputs, it only changes the geometry which is an important factor in the data processing described in Section 3.4. The new grid dimension were 2.7 × 2.7 meters instead of 4.5 × 4.5 meters.

Figure 4: Location of the ARISTA Facility

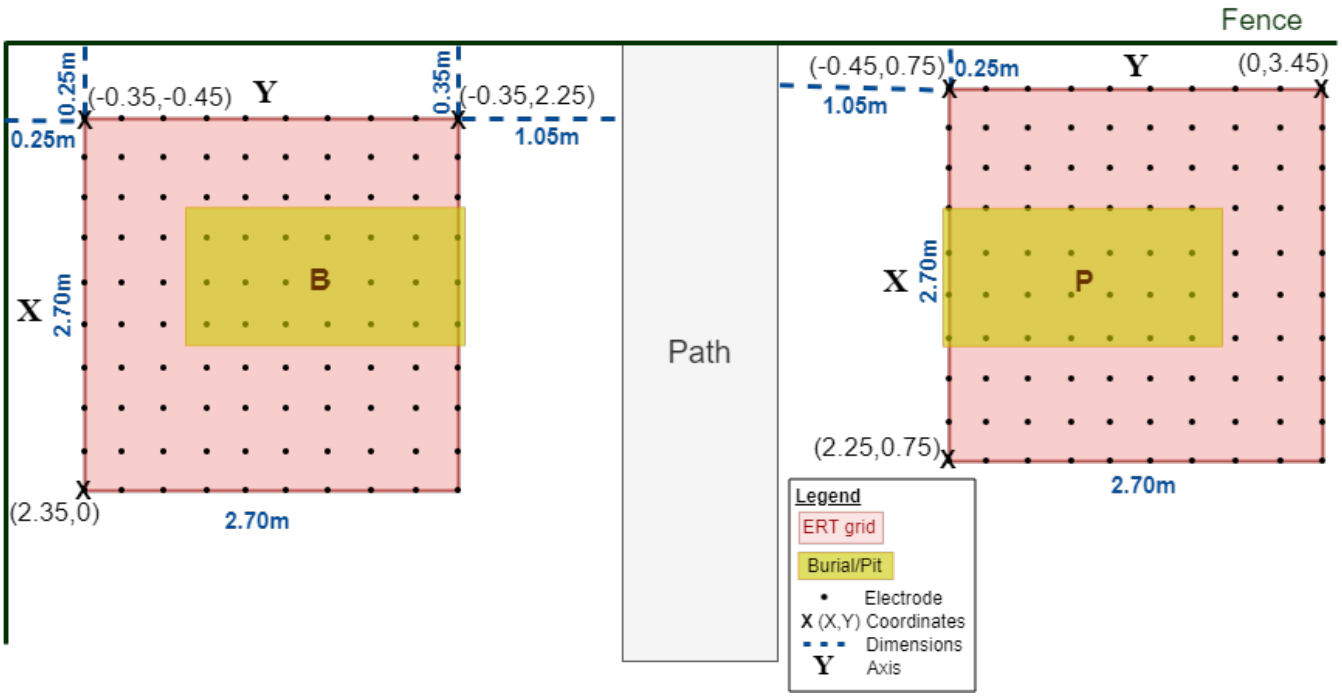

Figure 5: Location of the ARISTA Facility

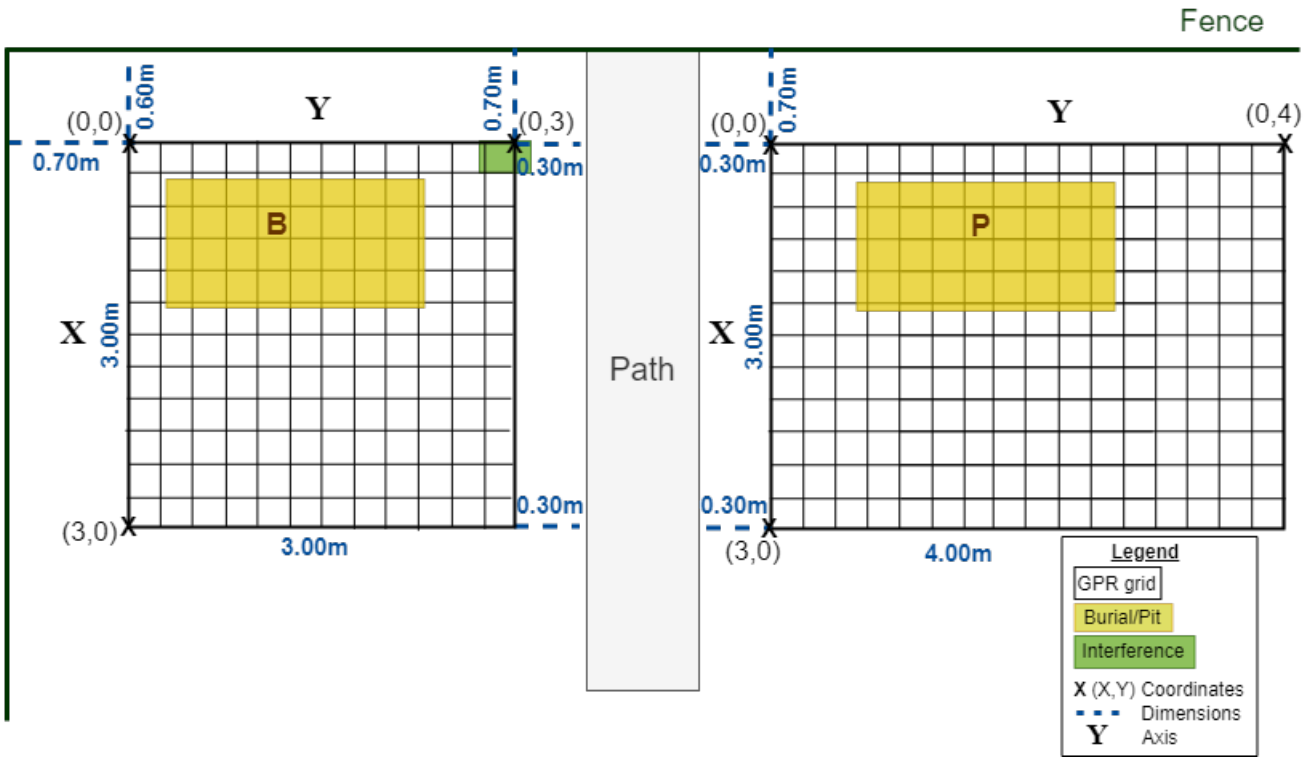

Figure 6: Location of the ARISTA Facility

3 Theory & Methods

3.1 General Approach

The ERT and GPR are each used in ways that are applicable to discovering a burial, and will complement each other in doing so. They are done over small areas, and the methods were designed to acquire enough data on the subsurface, to be able to compare and conclude on anomalies in the ground.

The ERT was split up into two methods. Firstly, a total of 20 2-dimensional dipole-dipole surveys were made. The first set of 10 were parallel and equally spaced with 0.25 meters, and the second set of 10 were as well but perpendicularly to the first set. This means that all intersections between the 2D surveys are at 90°. Using all information acquired in 2D, a 3D image was made. This was done with a 50V and a 100V injection potential, and for each potential a normal and a reciprocal measurement was done. In this context the term reciprocal means switching the current and the potential electrodes, meaning the electrodes which measured the potential will inject the current in the reciprocal measurement, and vice versa. The second method was directly 3D, where 8 sets of electrodes were selected to perform the current injection, and combinations of surrounding electrodes at a certain distance were made to measure the potential. Each measurement still consisted of 2 dipoles, but were not necessarily contained within the same 2D plane. For both methods the data sets were sorted, values with stacking errors over a certain threshold were filtered out, and then the data sets were inverted using forward modelling and an inversion scheme.

The GPR was used to create images in parallel lines with a spacing of 0.25 meters. This was done in two directions, which were perpendicular to each other.

This chapter describes the theory behind the ERT and the process to attain a 3D resistivity model, and also describes the geometries used to create electrode sequences for the data acquisition. A short description on GPR theory will be given, but will not be elaborated. For a comprehensive report on the GPR, the reader can refer to [5].

3.2 ERT Theory

Resistivity surveying can be done in both 2D or 3D, and is based on measuring the electric potential distribution of an injected current in the ground, and modelling the variations in resistance due to varying properties of materials in the ground. This geophysical method is based on Ohm's law, which states the following:

$$V = IR, \tag{1}$$

where V = electric potential [V], I = current [A] and R = resistance [Ω]. By injecting a direct current (DC) into the ground using two electrodes, the electrical potential can be measured at various locations using two other electrodes which do not carry a current. With each measurement, the resistance at various locations and depths can be determined. The injected current is determined by specifying an injection potential.

There are many ways of setting up the current and potential electrodes, and this research project will focus on employing the dipole-dipole array in two different geometries. First in 2D sections where all electrodes are always in line. These sections will be combined to create 3D models. Secondly measurements will be made directly in 3D, where the two dipoles are not on the same plane. The dipole-dipole array is shown in Figure 7.

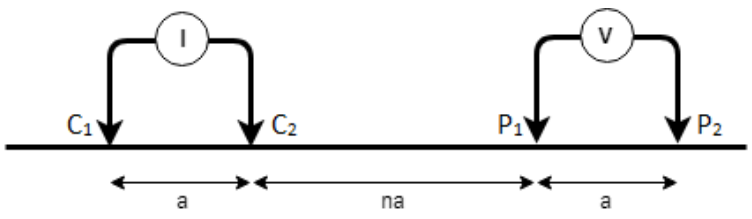

Figure 7: Dipole-dipole array

Each measurement results in an injection current value and a measured electric potential. To calculate the apparent resistivity, the following is done. We know from Ohm's law that the resistance R can be calculated using equation 1. We are however considering situations where the current is measured in a location at a finite distance from the potential measurement location. This distance is acknowledged within the geometric factor, k, which can be calculated using the following:

$$k = \frac{2\pi}{\frac{1}{r_{C_1P_1}} - \frac{1}{r_{C_1P_2}} - \frac{1}{r_{C_2P_1}} + \frac{1}{r_{C_2P_2}}}, \tag{2}$$

where $r_{C_iP_j}$ denotes the distance between current electrode i and potential electrode j. This formula is a general formula for the geometric factor of any 4 electrode array [15]. The apparent resistivity can then be calculated with the following:

$$\rho_a = \frac{V}{I}k, \tag{3}$$

where ρ_a is in ohmm. The term apparent resistivity means the resistivity a homogeneous earth would need to give the same potential measurements for the corresponding injected current [14]. These values do not acknowledge variations in resistivity, they assume the ground over which the measurement is done is completely homogeneous. These variations are found through combining all data and implementing an inversion scheme, which results in a true resistivity model of the ground.

3.3 Data Processing

The first step of the data processing was to invert the 50 V and 100 V normal/reciprocal data sets. To do this, the data was first filtered to remove errors of a certain size,. These errors are a result of automatic repetition (stacking) of the measurements, which is done in the IRIS. Along with this, any negative resistivity values were removed. Text files were then made which included the number of electrodes, their coordinates in (x, y, z), the number of measurements, the electrode sequences and their corresponding value of apparent resistivity that was calculated by incorporating the geometric factor. An example of this text file is given in the appendix. BERT then inverts the data and using ParaView the 3D models can be viewed. This resulted in 4 separate models.

To compare these 4 data sets, the following was done. For each voltage, the normal and the reciprocal data sets were visualized by plotting. These are all shown in the appendix. From these plots, any extreme deviations in the data could be analyzed. Ideally, there should be no differences between the normal and reciprocal data sets. However, due to the presence of telluric currents, deviations can be expected. These are natural or man made electrical currents in the ground [8], which cause 'noise' in the data. A new data set was then made with the averages between the normal and the reciprocal, and the deviation between the average and the data sets was calculated as a percentage of the average value. This resulted in a data set that included errors. Both data sets were then filtered to remove negative resistivity values, text files were made and the inversion was run. The same was then repeated, instead now the average result from the two 50V data sets was compared to that of the 100V data sets. This resulted in one final model for that specific grid.

The reason why this was done was because in theory, referring to Ohm's law (equation 1), a change in voltage should result in a proportional change in current, since the resistance of the ground should not change given constant conditions. If the data sets deviate by sufficient amounts, then this could be a sign of issues during acquisition.

This process was done for the data from the TU Delft site, the burial site and the non-burial site. The 3D out of plane measurements were only filtered to remove large stacking errors and negative values. The same type of text files were made and were input into BERT to complete the inversion.

3.4 Inversion Theory

Processing the resistivity survey data involves steps which are implemented in a program called Boundless Electrical Resistivity Tomography (BERT), written by Thomas Günther and Carsten Rücker [4]. This

section will explain the theory behind the inversion implementation, and how it is used for this specific application.

The first step in the inversion process is forward modelling of the data. A mesh was created that represents the volume of ground we want to model. The X and Y dimensions were based on the electrode grid, and the depth (Z dimension) was based on the raw data, the deepest measurement. The mesh was divided up into identical cubes, whose dimensions were found by taking the square of the electrode spacing as the X and Y dimension, and dividing this in half for the Z dimension. For example, if our electrode spacing is 0.5 meters, each cube is $0.25 \times 0.25 \times 0.125$ meters. In a mesh that is $4.5 \times 4.5 \times 1.25$ meters, we would have 3240 cubes. In this model, the resistivity in each cube will be homogeneous, meaning that this is also a measure of the resolution.

At first, the ground was assumed to have a homogeneous resistivity distribution. An average resistivity value was calculated from the input data, and this value was assigned to every cube within the mesh. The measurements from the IRIS were then simulated within the program, to form a data set such as the one achieved during the survey. This simulated data set was found using the following equation:

$$\nabla \cdot (\frac{\nabla V}{\rho}) = -\nabla \cdot j, \tag{4}$$

where V = electrical potential [V], j = current density [$\frac{A}{m^2}$] and ρ = resistivity [Ωm] [1]. The program simulated an injected current, measured the potential difference, and calculates a resistivity just like explained above. In the very first simulated data set, the values should all be identical since the resistivity is homogeneous.

Subsequently the simulated data set was compared to the actual data set through the method of least squares. This is known as the inversion, and it requires iterative steps to end up at the final result. The goal is to minimize the function ϕ, which is defined as:

$$\Phi = \Phi_d + \lambda \Phi_m. \tag{5}$$

Here, Φ_d is called the data functional [2], which considers the actual measured data $\mathbf{d}$ and the response of the model to the simulated data $\mathbf{f}(\mathbf{m})$. It is defined by the following equation:

$$\Phi_d(\mathbf{m}) = \sum_{i=1}^{N} \left| \frac{d_i - f_i(\mathbf{m})}{\epsilon_i} \right|^2 = \|\mathbf{D}(\mathbf{d} - \mathbf{f}(\mathbf{m})\|_2^2, \tag{6}$$

where $\mathbf{D}$ is a square matrix with dimensions equal to data length (N), and the diagonal is made up of the reciprocals of the corresponding measurement errors. Measurements with large errors will be assigned smaller weights in the inversion process, and vice versa. The data functional incorporates the least squares method, where in each iteration, new simulated data is calculated, which changes the model response and gradually minimizes Φ_d.

This process of minimizing is however considered 'ill-posed', as it simulates a model that is much more intricate than the length of data it is based on. Therefore the second term in the overall function is introduced:

$$\lambda \Phi_m = \lambda \left\| \mathbf{C}(\mathbf{m} - \mathbf{m^0}) \right\|_2^2. \tag{7}$$

$\mathbf{C}$ is again a square matrix whose dimensions are based on the model space. Each value in this matrix represents the correlation between two values in $\mathbf{m}$. For example, $C_{1,2}$ will be close to 1, since two adjacent cubes in the mesh can have high correlation, while $C_{1,2000}$ will be low since these are at a substantial distance from each other. $\mathbf{C}$ is therefore the smoothness matrix. λ is the weight that the smoothness matrix is assigned. A value of $\lambda = 2$ is used for the inversions done in this study, because the barrels are not very big relative to the electrode spacing, therefore any changes in resistivity over small areas should not be smoothed out. However, this could over fit the data such that very small anomalies become too visible. Finally, $\mathbf{m^0}$ is the model space of the very first simulated model, and the least squares principle is applied to the difference between each simulated model and the original model.

Combining the data and the model functional, iterations are performed to achieve a model space $\mathbf{m}$ that is as close to the actual data as possible, while maintaining a relationship with an initial model.

3.5 Acquisition Geometries

3.5.1 2D dipole-dipole geometry

A total of 100 electrodes were used to make a 10×10 electrode grid. All electrodes were then connected in one line using a zig-zag pattern as shown in Figure 8. Because of this, the numbering of the electrodes was also in a zig-zag order, which is important for the array inputs. An important thing to note is that referring to Figure 2, electrode 1 is at $(5.45, -0.20)$ and electrode 10 is at $(0.95, -0.20)$.

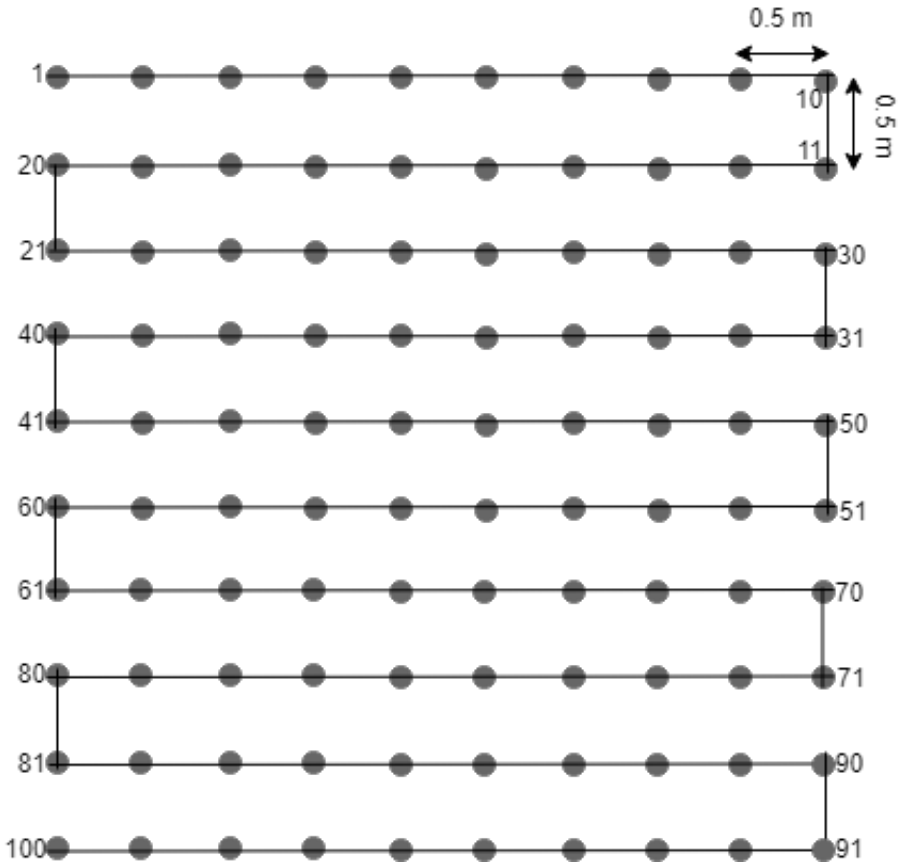

Figure 8: ERT Grid setup

A plan was uploaded to the IRIS main box, with a list of electrode configurations. Using the dipole-dipole array, configurations were made by essentially working in 2-D, taking each horizontal and vertical line of electrodes and starting off with the first two as current carrying. Figure 9 shows a few of the combinations used per line. The distance of the dipoles was increased, until the combination did not fit within the 10 electrodes.

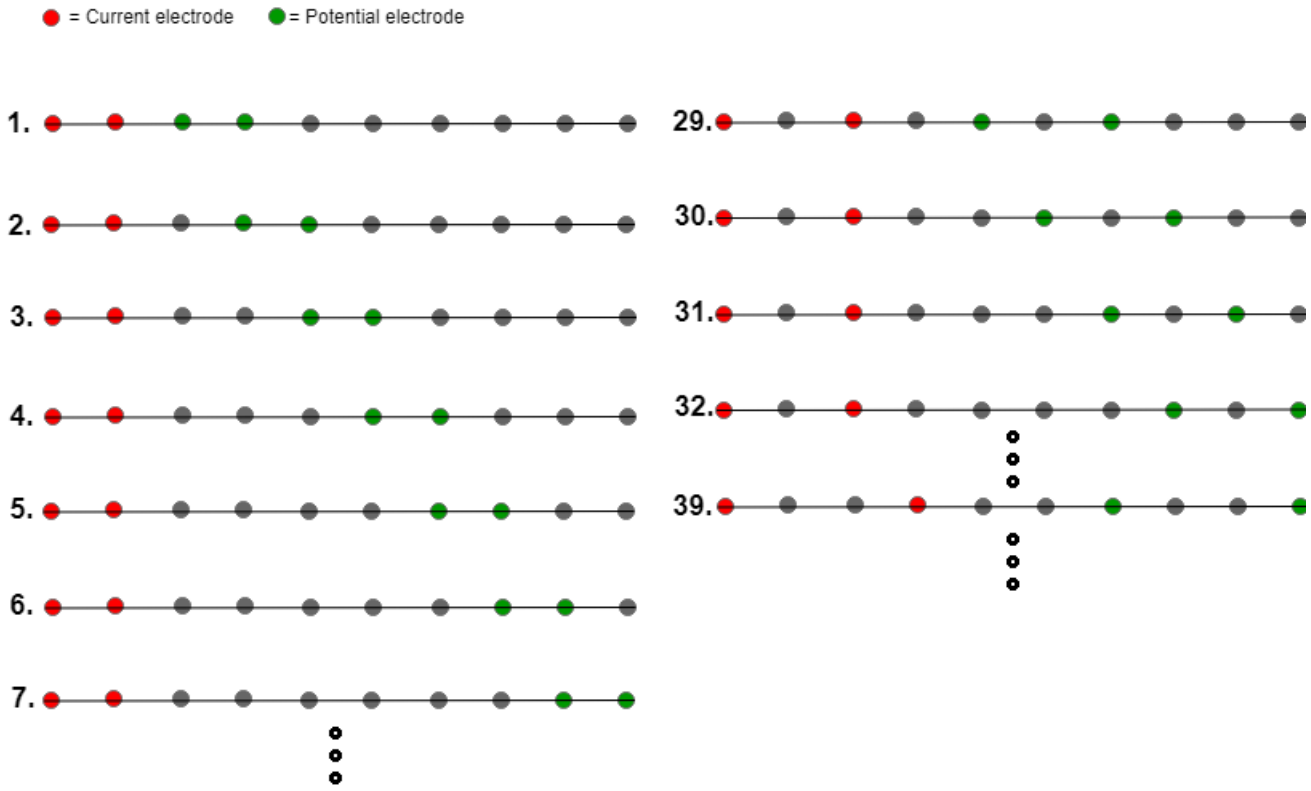

Figure 9: ERT array sequences for 2D dipole-dipole geometry. Only 12 of the 700 are shown, using the first 10 electrodes.

Using this method of creating configurations, the list shown in table 3 was made, and had a total of 700 configurations. This total measurement was then done 4 times, one with 50 V, with 100 V, and then again with 50 and 100 V but then the reciprocal version, where the current and potential electrodes were switched.

The 2D dipole-dipole method was performed at both sites described in sites section 2. The original 0.5 meter electrode spacing shown in figure 8 was used at the TU Delft site, but at the ARISTA facility in Amsterdam a spacing of 0.3 meters was used due to spacial constraints. However this does not change the electrode numbering, or the array inputs, it only changes the geometry which is an important factor in the data processing described in section 3.4. The new grid dimension were 2.7 $\times$ 2.7 meters instead of 4.5 $\times$ 4.5.

3.5.2 3D dipole-dipole out of plane

Creating an actual 3D model has endless possibilities of combinations of electrodes. While designing this, various combinations were made and through trial-and-error the following design was made in Matlab™. 8 electrode pairs where chosen around the outer edge of the grid. These pairs are shown in figure 10. Each pair was isolated and the midpoint was determined. Using this point, two concentric circles were made, one with a radius of 3 meters and the other with 6 meters. All individual electrodes that fell within this range where then used to make combinations of 2, which where set as all potential electrode pair possibilities. Figures 11 and 12 show these concentric circles for two of the 8 current electrode pairs. The green boundaries show the range from 3 - 6 meters.

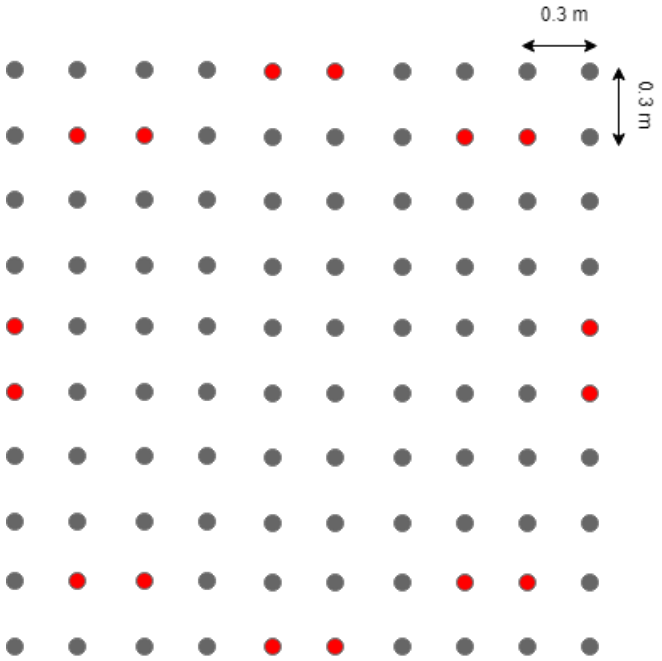

Figure 10: 8 electrode pairs chosen for the detailed configuration

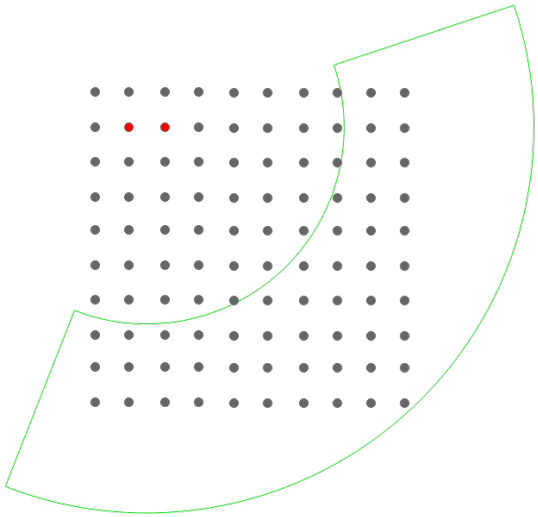

Figure 11: Concentric circle for electrode pair 19 18

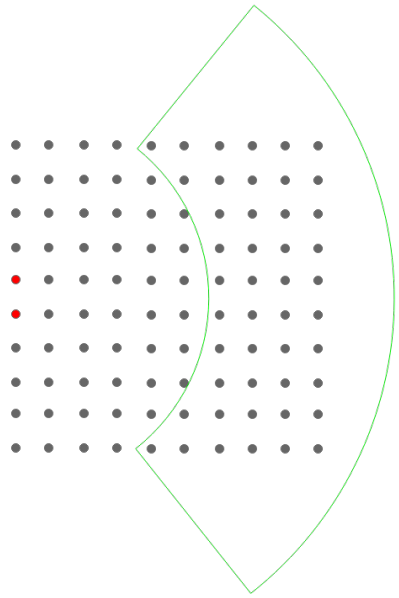

Figure 12: Concentric circle for electrode pair 41 60

Multiple factors were considered when building this configuration plan. The two most important were related to processing time and measurement reach. The more measurements present within one run, the longer it will take. With the 700 measurements it took about 15 minutes to complete, therefore in total the 4 runs took around an hour. The second configuration plan came out to a total of 5292 measurements, and took a total of 4.5 hours. Due to time constraints it was decided that around 5000 measurements was the maximum. Concerning the reach, the objective was to get the midpoint between current and potential pair of all measurements close to the center of the grid. This is why the range from 3 - 6 meters was used, and when performing the survey on the burial, the known location of the body was aimed to be in the center of the grid.

3.6 GPR

A GPR is an instrument which can send a high frequency electromagnetic pulse into the ground, which is then reflected in the ground and picked up by the receiving part of the GPR. Reflections occur because of

changes in the dielectric properties of the soil [14]. When an anomaly is present, a reflection will show up and this can give information on the location and depth of the anomaly. These surveys can be done in 2D straight lines, by pulling the GPR over the ground. An odometer rolls over the ground and triggers the transmitter to send pulses. Frequencies of 250, 500 and 1000 MHz can be used, and for this it was chosen to use the 250MHz because the research done last year showed the higher frequencies picked up too much noise from tree roots.

The GPR was performed in parallel lines going in 2 directions which are perpendicular to each other. Referring to Figure 2 in Section 2.1, the common offset method was done in the following way: The first measurement was taken in a line from $(0, 5.25)$ to $(0, 0)$, where this line was on the center of the GPR cart. An important fact to mention is that at the start of each measurement, the GPR was halfway across the $X = 5.25$ line, meaning that the transmitter was on the right side of $X = 5.25$ and the receiver on the left side. After the first measurement, the GPR was then picked up and brought back to $X = 5.25$ and a new measurement was made from $(0.25, 5.25)$ to $(0.25, 0)$. This was continued with increments of 0.25 m until the last line on $Y = 4.5$. Measurements were then made parallel to the previous, starting with a line from $(5.25, 4.5)$ to $(5.25, 0)$. Again with increments of 0.25 m, the lines shifted towards the left until the last one from $(0, 4.5)$ to $(0, 0)$.
This method can be applied to any grid of any dimension or size, and for this project a spacing of 0.25 meters was kept constant.

4 Results

4.1 TU Delft

4.1.1 2D dipole-dipole

First the raw data can be analyzed. This is done by looking at the 2D pseudo sections at the depth the barrels are expected to be. These pseudo sections are shown in Figures 13 through 16. These show very high similarity which is favourable, and no sudden peaks or extremely high values are present. It is therefore expected that the true resistivity models will be similar.

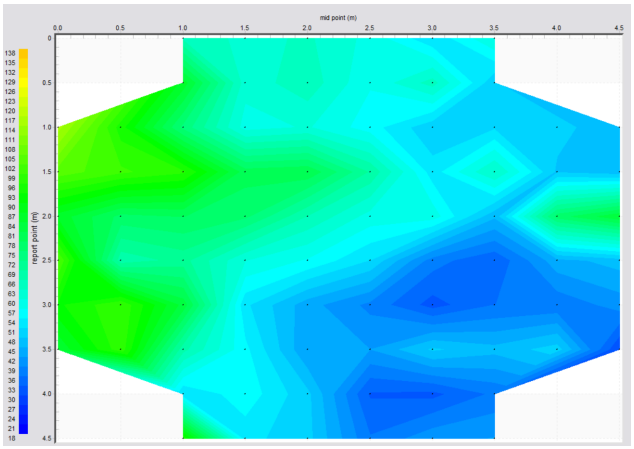

Figure 13: 2D pseudo section of raw data at approximately 0.25 meters depth for TU Delft 50V normal

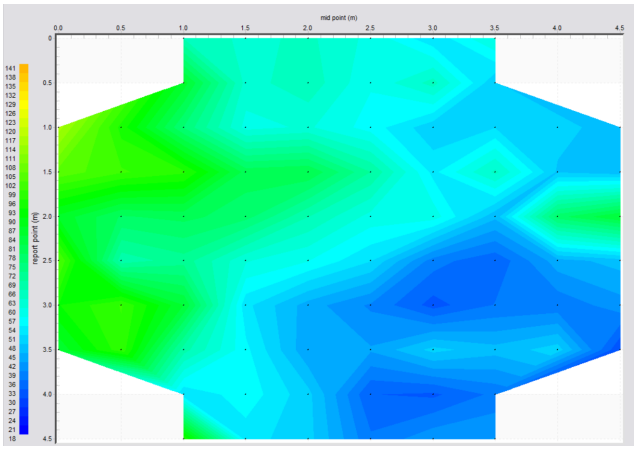

Figure 14: 2D pseudo section of raw data at approximately 0.25 meters depth for TU Delft 50V reciprocal

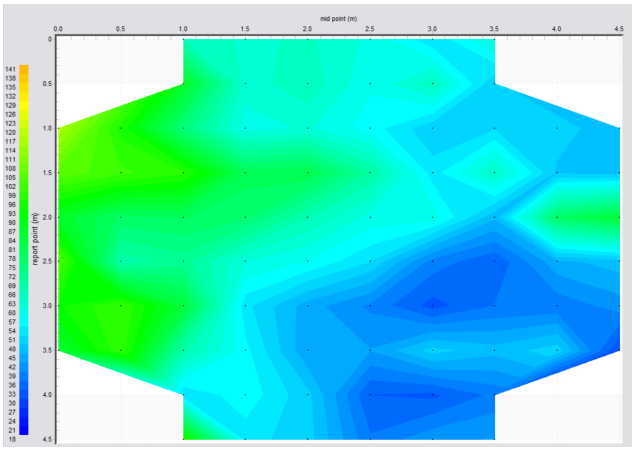

Figure 15: 2D pseudo section of raw data at approximately 0.25 meters depth for TU Delft 100V normal

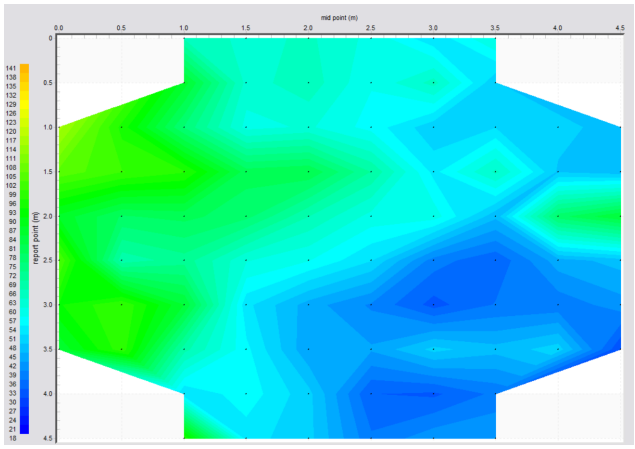

Figure 16: 2D pseudo section of raw data at approximately 0.25 meters depth for TU Delft 100V reciprocal

The following images show all 7 inverted models at the TU Delft site. The barrels are known to be buried in a pit with a depth of about 0.35 meters [6], therefore the models have been 'clipped' to show the horizontal plane at 0.25 meter depth. All resistivity models are viewed in ParaView which uses the coordinates based on the electrodes. Therefore to clarify, the origin $(0, 0)$ shown in all models is located at $(5.5, -0.20)$ in the coordinate plane in Figure 2. And $(0, 4.5)$ in the model is located at $(0.95, -0.20)$. Figure 36 in the appendix shows the direction in which the models are viewed.

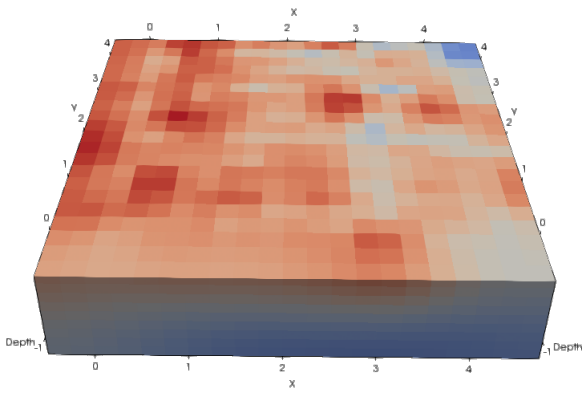

Figure 17: TU Delft 50V normal

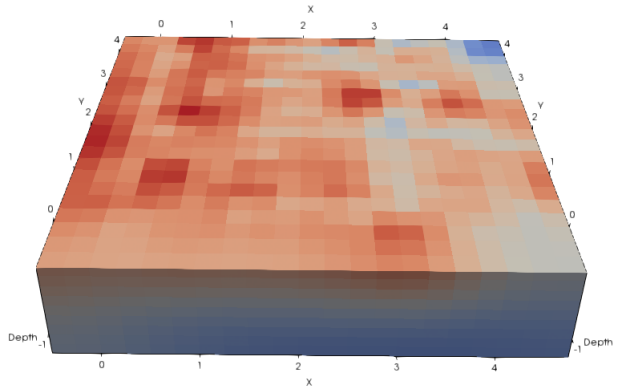

Figure 18: TU Delft 50V reciprocal

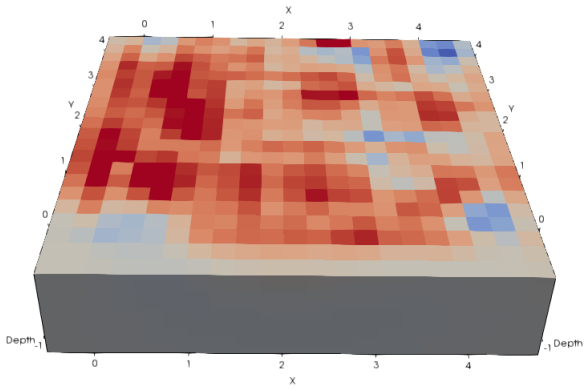

Figure 21: TU Delft 50V combined

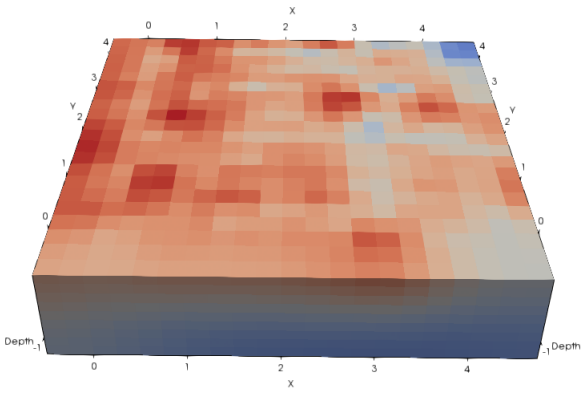

Figure 19: TU Delft 100V normal

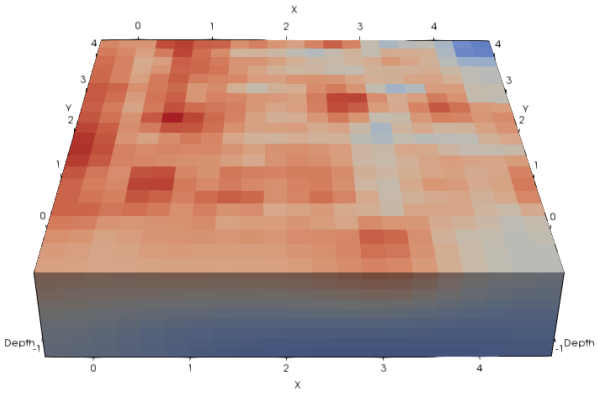

Figure 20: TU Delft 100V reciprocal

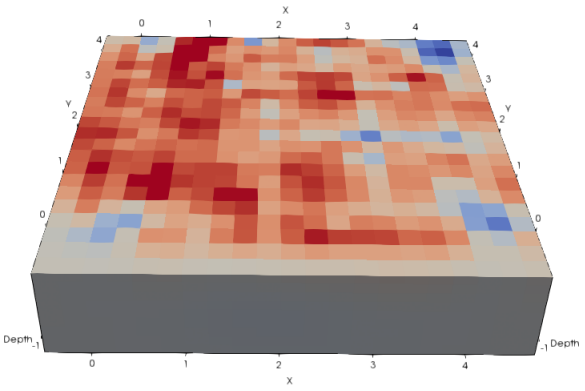

Figure 22: TU Delft 100V combined

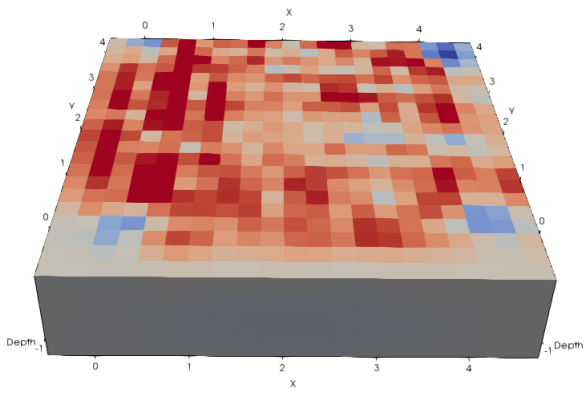

Figure 23: TU Delft all combined

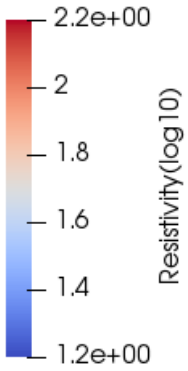

Figure 24: Colour scale used for TU Delft resistivity models

The models shown in Figures 17 to 20 seem almost identical, with very few differences. This is a positive result because it means the data sets did not differ by much, leading to low errors. These errors are shown in the appendix in Figures 38 and 40. The models in Figures 21 and 22 are however a bit different compared to the first 4, which is a result of the error weighting from comparing the data sets. The same can be said about Figure 23. One thing to notice is that it seems as if comparing the data sets and using averages and error weightings has cause some lithology to be lost. For example, in the 50V normal model (Figure 17) there is lateral change in resistivity, where the ground becomes less resistive as depth increases. This lateral variability is lost in the combined models.

Because of the similarity between the four models in Figures 17 - 20, we can isolate the 50V normal and analyze with this model. Using Figure 3 to give an idea of the potential locations of the barrels, the following anomaly locations could be of interest:

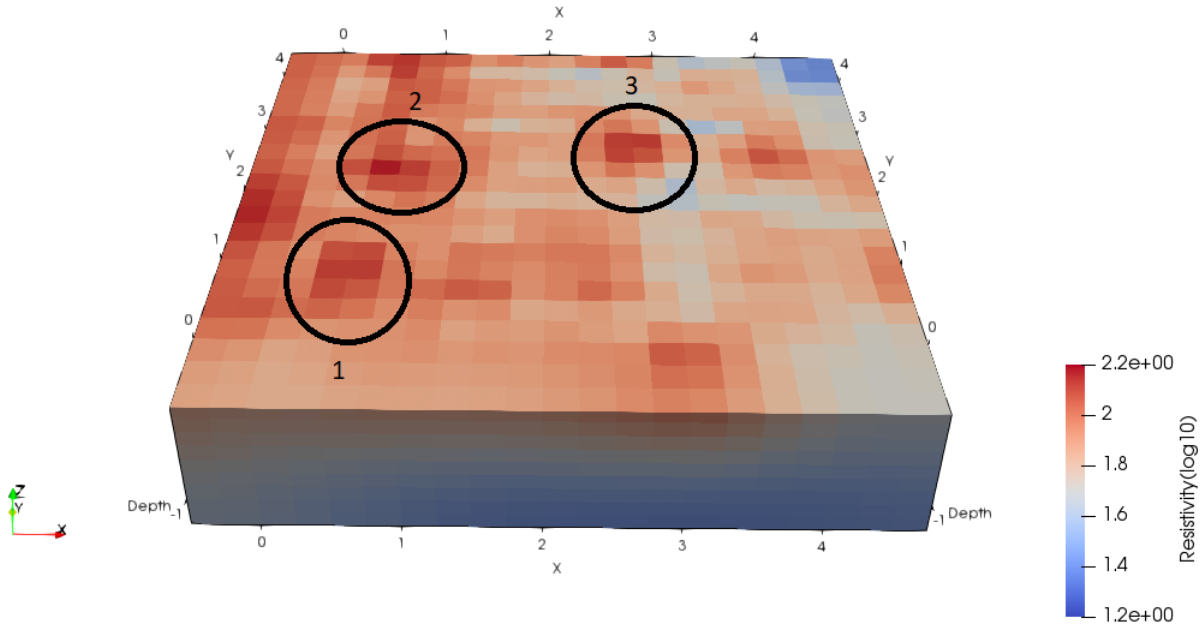

Figure 25: Visible anomalies in the 50V normal model at TU Delft site

To analyze this further, the GPR data around these location can be used to compare. Figures 26 through 33 show these radargrams and their location. The locations of each radargram is based on the coordinate

system shown in Figure 2.

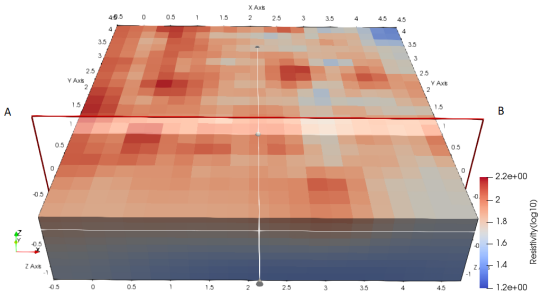

Figure 26: Location of radargram at $X = 4.5$ m

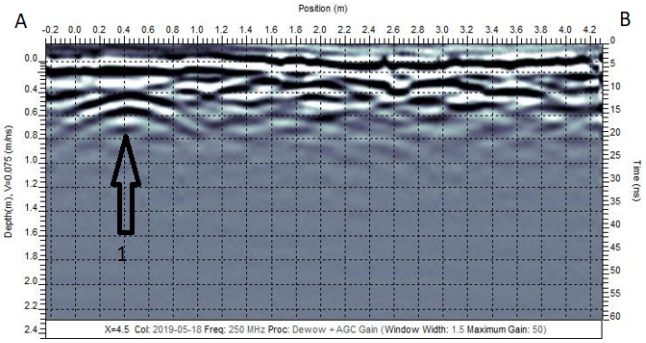

Figure 27: Radargram at $X = 4.5$ m. Arrow labelled '1' shows the location of anomaly 1.

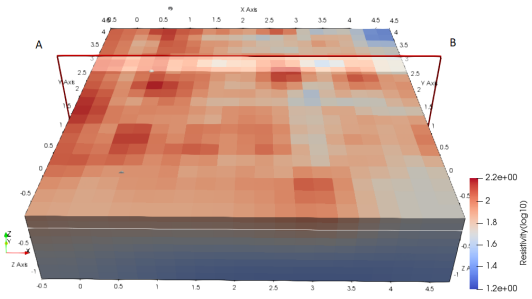

Figure 28: Location of radargram at $X = 3$ m

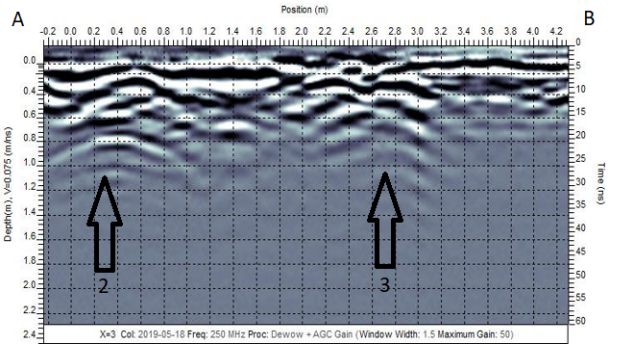

Figure 29: Radargram at $X = 3$ m. Arrows labelled '2' and '3' show the locations of anomalies 2 and 3 respectively.

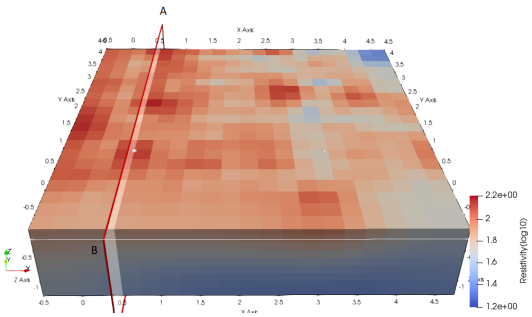

Figure 30: Location of radargram at $Y = 0.25$ m

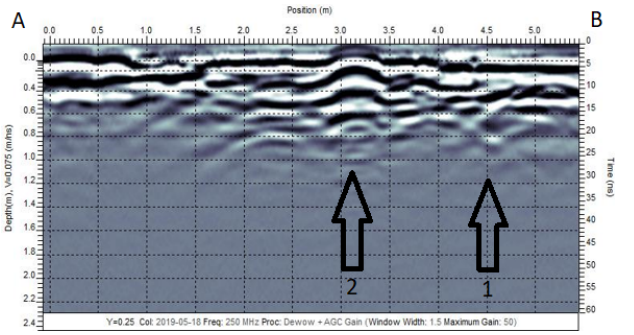

Figure 31: Radargram at $Y = 0.25$ m. Arrows labelled '1' and '2' show the locations of anomaly 1 and 2 respectively.

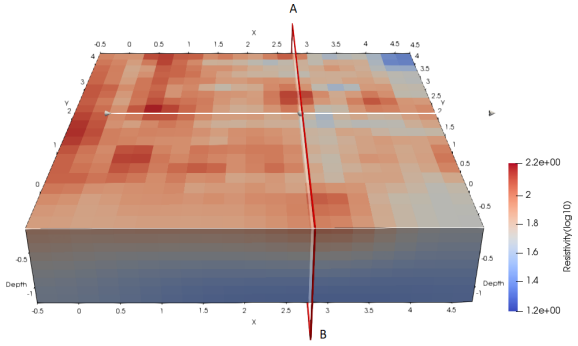

Figure 32: Location of radargram at $Y = 2.5$ m

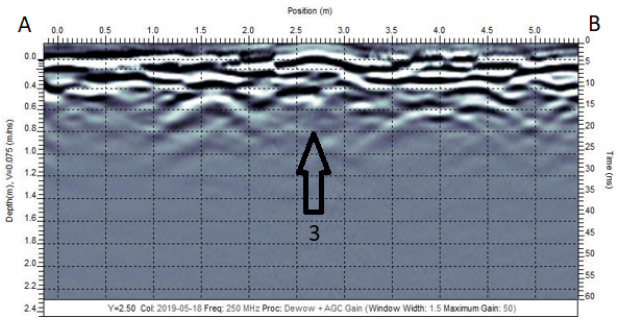

Figure 33: Radargram at $Y = 2.5$ m. Arrow labelled '3' shows the location of anomaly 3.

Each arrow is located at the position where the anomaly is seen in the ERT data. The arrows are labelled with the anomaly number from Figure 25. Starting with the first anomaly, in Figure 27 a clear reflection can be seen at this position. This gives way that the empty barrel could be located here, if comparing to the barrel locations in Figure 3, however the reflection in Figure 31 is not very clear, but could be disturbed by noise. The second anomaly also gives a clear reflection in Figures 29 and 31. Comparing this to the barrel locations, it seems as if they are too 'in line' to be the empty and the rod filled barrel, but this depends on the orientation of the coordinate grid. Say our grid is rotated a bit anti-clockwise, then they would not be in line. The third anomaly causes a clear reflection shown in Figure 29, and also in Figure 33.

These same anomalies can be seen in the combined models in Figures 21 and 23, but in the combined model for 100V shown in Figure 22 the three anomalies do not stand out as much anymore.

The results from the facility in Amsterdam are included in the appendix due to their uncertainty. This is only done for the 2D dipole-dipole measurements over the burial site, the remaining models are not shown because these are all unrealistic resisitivity models.

5 Discussion

This section explains the issues encountered during data acquisition and processing, and a possible solution/recommendation for a continuation of this project is described.

5.1 Coordinates of TU Delft site

Assumptions had to be made regarding the coordinates of the buried barrels, due to the absence of exact coordinates of the TU Delft site. Conclusions could still be made, but for further research a possible solution to this problem is to set up an allocated site, which is made for this specific research. The boundaries of the site could then be explicitly defined, and a variety of objects could be buried for long term research. These locations would then have to be clearly defined. This site would then only be open to students doing research there, to ensure no interference with the buried objects.

5.2 Burial position at facility

Referring to figure 5 or 6, it can be seen that the burial lies about 1 meter away from a metal fence. For entomology or remote sensing purposes this should not be an issue, but for geophysical studies this can be an interference. The metal fence continues for 1 meter into the ground. Along with this, in figure 6 the green rectangle at $(0, 3)$ shows the location of a metal plate, which looks like an opening for drainage. These metal anomalies in the ground show up as very strong reflections in the GPR data, making it difficult to detect any other anomalies. Whether the fence or the metal plate interfere with ERT results is unknown, because of the faulty data which is explained below. If extensive research on detecting clandestine graves with geophysical tools is wanted, then perhaps a cadaver (or more) could be placed at the center of the facility, or at a location with minimal disturbances around it. This is of course easier said than done, but it would allow for much better results, and further progression in this field of study.

5.3 Faulty ERT Data

The ERT results at the TU Delft and the Amsterdam facility site were acquired on 3 separate days over the course of about two weeks. While analyzing the TU Delft raw data, no strange measurements could be seen and the range of apparent resistivity values was about 18 - 138 ohm.m. The measurements from Amsterdam ranged from about 400 ohm.m to 6000 ohm.m, and in another data set it even went from -7000 ohm.m to 6000 ohm.m. Initially it was assumed that this was due to bad contact resistances. Appropriate values for the contact resistance are around 2 kOhm, and preferably the contact resistance is around the same value for all electrodes. It was however challenging to achieve low values, because of the presence of the body which we did not want to puncture. Had these resistances been the issue, then a possible solution would be to make the ground wet with water or a salt solution. Moist soil is more conductive and therefore gives a better contact resistance. This was however not allowed, because the moisture content was also being studied around the cadaver, and introducing water to the ground would meddle with their results. Like mentioned before, having a cadaver specifically for geophysical studies would allow for measures to be taken to get better contact resistances.

It is not clear however if the contact resistances are the only issue, because a few weeks after the data acquisition in Amsterdam a problem with the IRIS instrument was discovered. This problem resulted in resistivity measurements ranging from low values to extremely high values, which can also be seen in the data from Amsterdam. This makes the data from Amsterdam very uncertain, and although the data can still be inverted, it is difficult to make conclusions because the accuracy is very uncertain.

5.4 GPR Frequencies

The 250 MHz GPR was used, and this choice was made based on the conclusions from last years research. Although this was the right decision for the soil conditions at the TU Delft site, a higher frequency could have been used at the site in Amsterdam because the ground there was made up of sand.

5.5 Recommendations for future research

The following is a list of recommendations for a continuation of this research, based on issues or limitations encountered during this project.

Firstly, time constraints were the greatest limiting factor. 7 weeks were available to do all planning, acquisition and processing. This gave little room for mistakes or issues. Had there been more time, a second visit to the facility in Amsterdam would have been possible with repaired IRIS equipment. Therefore this may be a better thesis project if there is more time available, for example if someone is doing this earlier in the academic year and has 10 weeks. Or perhaps this could be the topic for a masters thesis. In that case the research can be much more extensive. Another time related recommendation is to practice performing ERT surveys beforehand, to be able to do the surveys at the very beginning to make room for any surveys that need to be repeated. Practice is essential when working with the ERT.

Another way to be more time efficient is to learn how to do the data processing at the very beginning. Once a script is written in Matlab that can calculate the geometric factors, the apparent resistivities and place everything in a text file, this can then easily be done on site and inverted. The inversion does not take very long, and then the data and the results can be analyzed on site and any issues can be resolved immediately.

The 2D dipole-dipole method makes use of sequences that combine the same 4 electrodes only once. For example, there was only one measurement which employed electrode 1, 2, 3 and 4. To use the same method but achieve more measurements, the current or the potential electrodes could be switched. The following table shows an example of all the possible dipole-dipole combinations that can be made using the first four electrodes.

Config.	Current electrode 1	Current electrode 2	Potential electrode 1	Potential electrode 2
1.	1	2	3	4
2.	2	1	3	4
3.	2	1	4	3
4.	1	2	4	3
5.	3	4	1	2
6.	4	3	1	2
7.	4	3	2	1
8.	3	4	2	1

Table 2: Possible combinations of 4 electrodes in dipole-dipole array

Concerning the data processing, paying attention to how the IRIS interprets the input coordinates can save time. The plan that is uploaded to the IRIS main box includes the coordinates of each electrode number, and the electrode sequences for each measurement. After processing all the data and completing inversions, it was discovered that the IRIS had interpreted the input coordinates in a different way than was intended. Along with this, the reciprocal measurements were ordered differently than the normal. Due to the lack of experience in working with the IRIS, this was discovered quite late and lead to repeating the data processing and inversion. Paying attention to details like these can save time.

Concerning the GPR, a higher frequency should be used if further research is done at the facility in Amsterdam. Knowing now that high GPR frequencies work well with sandy soils, these can be tested at the facility in Amsterdam.

To test out the design for the 3D out of plane dipole-dipole survey, a simulation could be done with a generated data set. This could then be used to determine how well this design works and if any adjustments need to be made.

A final recommendation, which is briefly stated above under Section 5.1, is to set up a test site at or near the TU Delft campus that is explicitly made for this type of research. Various objects such as barrels,

but also plain metal rods, plastic bags or clothing bundles, anything that resembles forensic evidence can be buried here. This gives the opportunity to really practice working with the ERT and to see whether or not the measurement plan or the electrode spacing etc. works to detect the buried objects. At this site, a good comparison can be made between a 2D dipole-dipole method and a 3D out of plane method. Other arrays could also be tested to see whether these result in more accurate resistivity models.

6 Conclusion

The goal of this research project was to test the applicability of ERT as a geophysical tool in forensic investigations. The results at the TU Delft show clear anomalies with high resistances at three locations. The first anomaly shows a very clear reflection in the GPR radargram at X = 4.5 meters, yet in the radargram at Y = 0.25 meters this reflection is not as clear. The second anomaly shows very clear reflections in both the X = 3 meter and the Y = 0.25 meter radargrams. The third anomaly shows a reflection in the X = 3 meter radargram, but it shows a less prominent reflection in the Y = 2.5 meter radargram. It is known that there are 2 barrels buried in the ground, and when referring to the coordinates in Table 1 in combination with the ERT and GPR results it can be concluded that the empty barrel is at the location of anomaly 1, and the rod filled barrel is anomaly 3. Anomaly 2 could perhaps be a pipe in the ground, since this test site was directly next to a building.

The 2D dipole-dipole method proved to be successful in determining the location of the barrels. This method can be done quickly, and repeated many times within one day of fieldwork. There are many more combinations that can be made with this method which can result in more measurements.

Overall, the potential of ERT as a tool to locate object buried in the subsurface remains, and research within this field should be continued and extended to establish how these tools can advance forensic investigations.

References

[1] Günther, T., Rücker, C. and Spitzer, K. (2006a). Three-dimensional modelling and inversion of DC resistivity data incorporating topography I. Modelling. *Geophysical Journal International*, 166:495 505.

[2] Günther, T., Rücker, C. and Spitzer, K. (2006b). Three-dimensional modelling and inversion of DC resistivity data incorporating topography II. Inversion. *Geophysical Journal International*, 166:506 – 517.

[3] A. Williams, C.J. Rogers, J.P. Cassella (2019). Why does the uk need a human taphonomy facility? *Forensic Science International*, 296:74–79.

[4] Günther, T., Rücker, C. (2011). Boundless electrical resistivity tomography bert 2 - the user tutorial.

[5] Hansen, F. (2019). The use of common-offset and multiple-offset gpr methods for forensic investigations.

[6] Harms, K. (2018). GPR and EM Responses to Buried Clandestine Forensic Objects in Wet and Dry Soil Conditions.

[7] Jones, G. (2008). Geophysical mapping of historic cemeteries. *Technical Briefs In historical archaeology*, 3:25–28.

[8] Louis J. Lanzerotti, G. P. G. (1986). *The Earth's Electrical Environment, Telluric Currents: The Natural Environment and Interactions With Man Made Systems*. National Academies.

[9] Rubio-Melendi, D., Gonzalez-Quirs, A., Roberts, D., Garca Garca, M. del C., Caunedo Domnguez, A., Pringle, J. K., Fernndez-lvarez, J. P. (2018). GPR and ERT detection and characterization of a mass burial, Spanish Civil War, Northern Spain. *Forensic Science International*, 287:e1 – e9.

[10] Sarris, A., Papadopoulos, N. (2012). Looking for graves: Geophysical prospection of cemeteries. *Conference on Cultural Heritage and New Technologies*, pages 1–13.

[11] Time and Date AS (2019). Climate and weather averages in amsterdam, netherlands.

[12] Vass, A. A. (2001). Beyong the grave - understanding human decomposition. *Microbiology Today*, 28:190 – 192.

[13] Vroom, A. (2018). The Potential of Geophysical Instruments as Tools for Forensic Searches.

[14] Wightman, E., Jalinoos, F., Sirles, P., Kanaan, H. (2003). Application of geophysical methods to highway related problems. Technical report.

[15] Zohdy, A. A. R. (1970). *Geometric Factors of Bipole-Dipole Arrays*.

A Appendix

A.1 Equipment

A.1.1 ERT Equipment

For electrical resistivity surveys, the TU Delft has an IRIS instrument which is available to students. The following list gives an overview of all components necessary for our ERT surveys, which are also partially shown in Figure 34:

- IRIS main control box
- IRIS external box
- Connecting cable between the two boxes
- 3 large batteries
- 3 cables, each for 36 connections
- 100 steel electrode rods
- 100 cable clips
- 6 battery cables
- IRIS wiconnect
- Fieldwork laptop

Figure 34: ERT equipment

A.1.2 GPR Equipment

For the GPR surveying the materials came in a set, called the PulseEKKO Pro from Sensors and Software. This was also provided by the TU Delft. It comes in various frequencies, namely 1000, 500 and 250 MHz. For this project it was decided to only use the 250 MHz as the 500 MHz resulted in too much noise. The following list shows all components used for this project.

- PulseEKKO Pro shielded transmitter box
- PulseEKKO Pro shielded receiver box
- Cart with handle for keeping the boxes in place and pulling them
- Odometer
- Two cables to connect transmitter and receiver to control unit
- Control unit and carrying device
- Small battery pack to power control unit

Figure 35: GPR equipment

A.2 Direction of view for TU Delft results

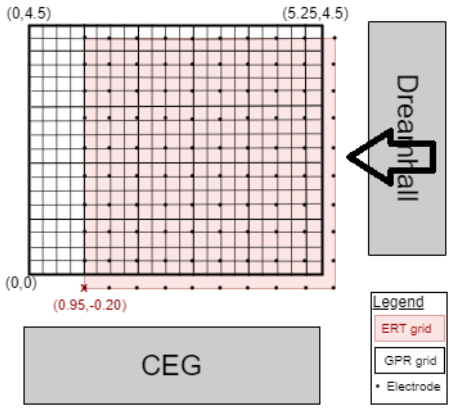

Figure 36: Arrow showing direction of view for TU Delft results

A.3 Array sequences for the 2D dipole-dipole geometry

Config.	Current electrode 1	Current electrode 2	Potential electrode 1	Potential electrode 2
1.	1	2	3	4
2.	1	2	4	5
3.	1	2	5	6
29.	1	3	5	7
30.	1	3	6	8
39.	1	4	7	10
40.	20	19	18	17
41.	20	19	17	16
42.	20	19	16	15
68.	20	18	16	14
69.	20	18	15	13
77.	20	17	14	11

Table 3: Example of electrode configurations from TU Delft grid plan. Only 12 of the 700 are shown here as an example, using the first 10 electrodes.

A.4 Text file input for BERT

The following text file shows the layout of the input for BERT. There were 100 electrodes, and the coordinates of the first 20 are shown. Then after filtering the data based on the stacking errors, 647 measurements remained. the columns a, b, m and n are the electrode indices. 'a' and 'b' are the current injection electrodes, and 'm' and 'n' are the potential electrodes. 'rhoa' stand for the apparent resistivity ρ_a. The first 20 measurements are shown.

100
x y z
0.0 0.0 0.0
0.0 0.5 0.0
0.0 1.0 0.0
0.0 1.5 0.0
0.0 2.0 0.0
0.0 2.5 0.0
0.0 3.0 0.0
0.0 3.5 0.0
0.0 4.0 0.0
0.0 4.5 0.0
0.5 0.0 0.0

0.5 0.5 0.0
0.5 1.0 0.0
0.5 1.5 0.0
0.5 2.0 0.0
0.5 2.5 0.0
0.5 3.0 0.0
0.5 3.5 0.0
0.5 4.0 0.0
0.5 4.5 0.0
647
a b m n rhoa
1.000000 11.000000 21.000000 31.000000 82.149983
1.000000 11.000000 31.000000 41.000000 65.325660
1.000000 11.000000 41.000000 51.000000 54.282803
1.000000 11.000000 51.000000 61.000000 46.193333
1.000000 11.000000 61.000000 71.000000 37.621488
1.000000 11.000000 71.000000 81.000000 30.097191
11.000000 21.000000 31.000000 41.000000 72.597264
11.000000 21.000000 41.000000 51.000000 62.068299
11.000000 21.000000 51.000000 61.000000 51.169410
11.000000 21.000000 61.000000 71.000000 39.829666
11.000000 21.000000 71.000000 81.000000 30.579703
11.000000 21.000000 81.000000 91.000000 28.941575
21.000000 31.000000 41.000000 51.000000 74.242025
21.000000 31.000000 51.000000 61.000000 63.443903
21.000000 31.000000 61.000000 71.000000 47.973626
21.000000 31.000000 71.000000 81.000000 34.703976
21.000000 31.000000 81.000000 91.000000 30.996931
31.000000 41.000000 51.000000 61.000000 75.250244
31.000000 41.000000 61.000000 71.000000 59.027745
31.000000 41.000000 71.000000 81.000000 41.051681

A.5 Data analysis plots

The following images show the apparent resistivity measurements in plots. Each plot includes 3 data sets, the normal, the reciprocal and the average between the two. The green line is the normal, blue is the reciprocal and red is the average between the two. The errors are the deviations between the average values and the corresponding data values.

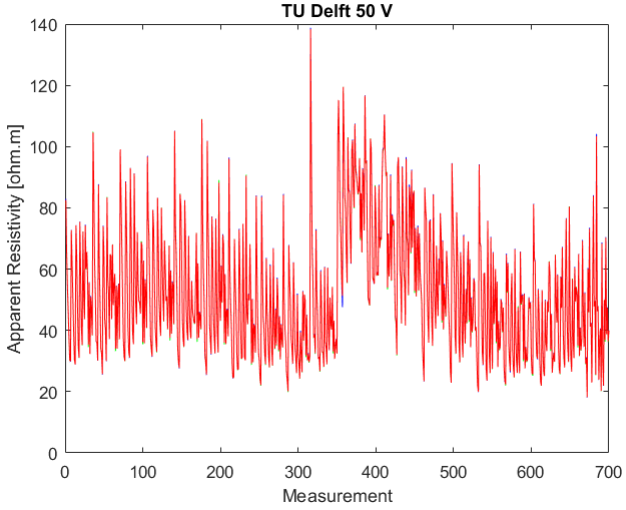

Figure 37: Data TU Delft 50V

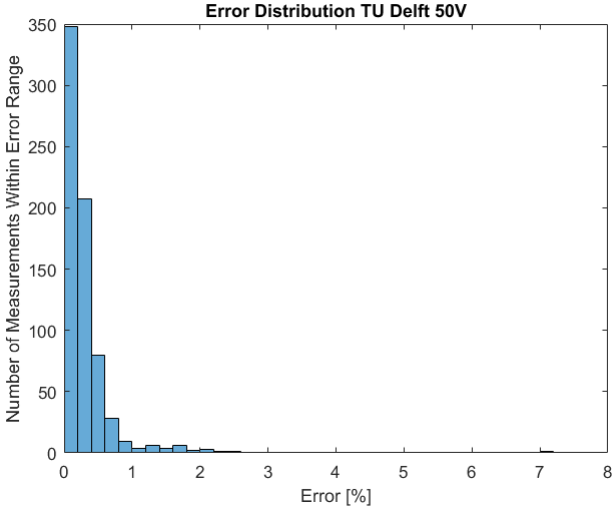

Figure 38: Errors TU Delft 50V

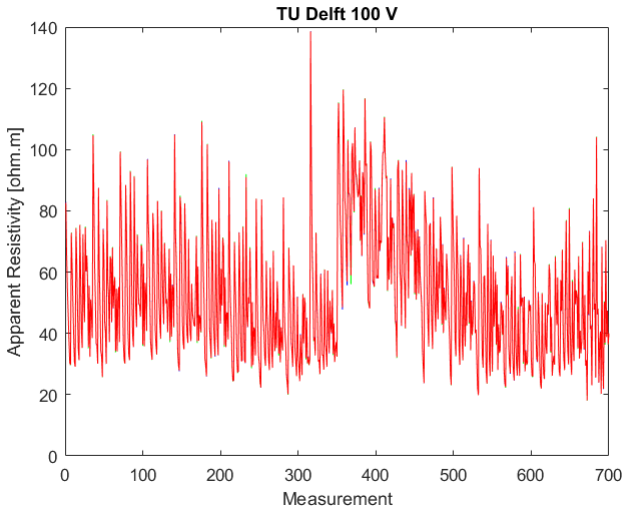

Figure 39: Data TU Delft 100V

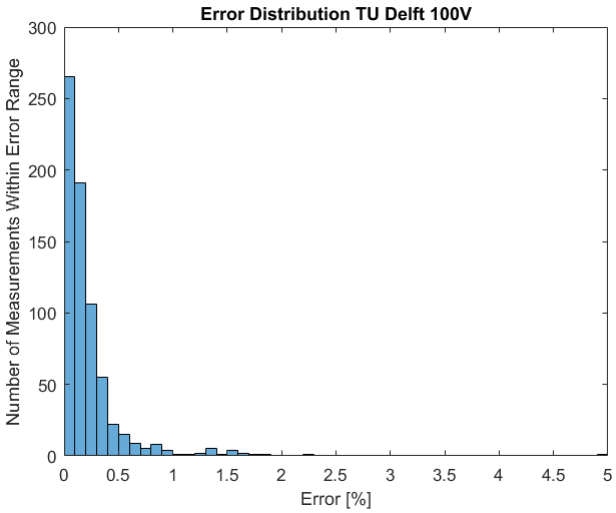

Figure 40: Errors TU Delft 100V

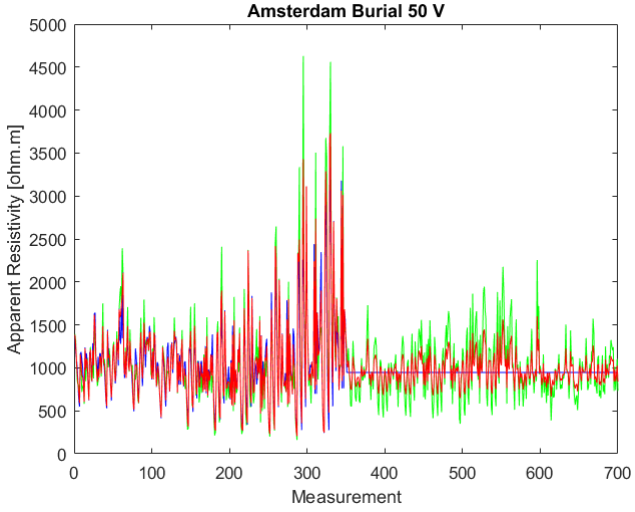

Figure 41: Data burial site 50V

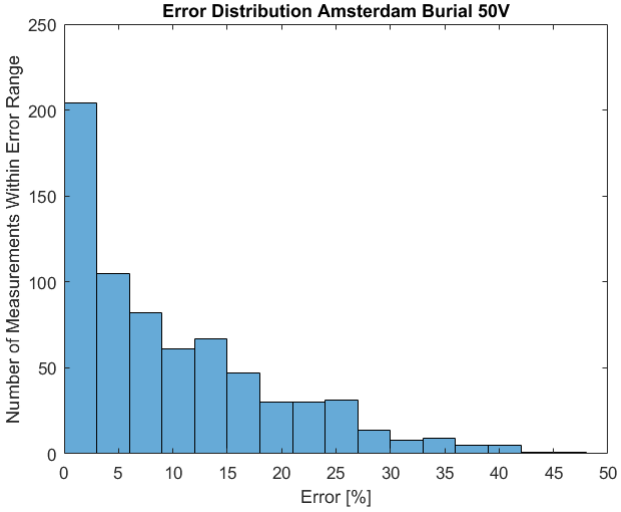

Figure 42: Errors burial 50V

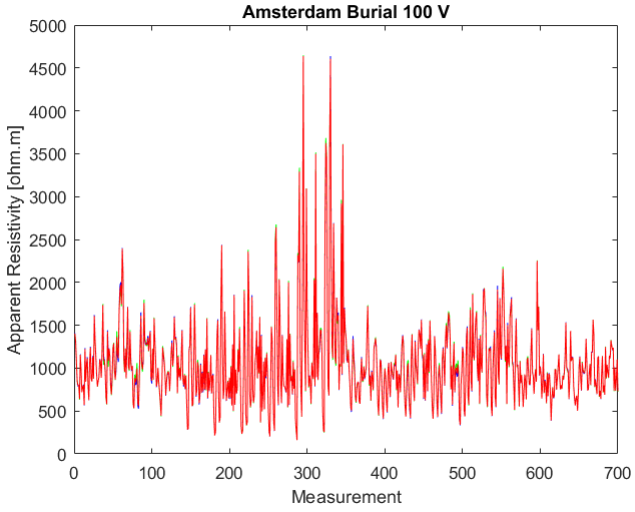

Figure 43: Data burial site 100V

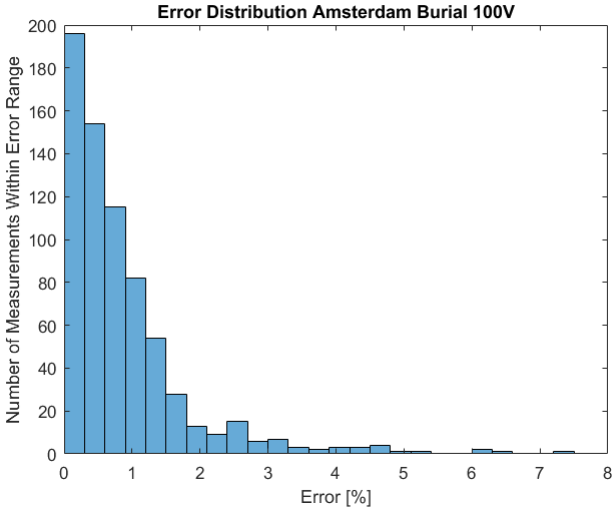

Figure 44: Errors burial 100V

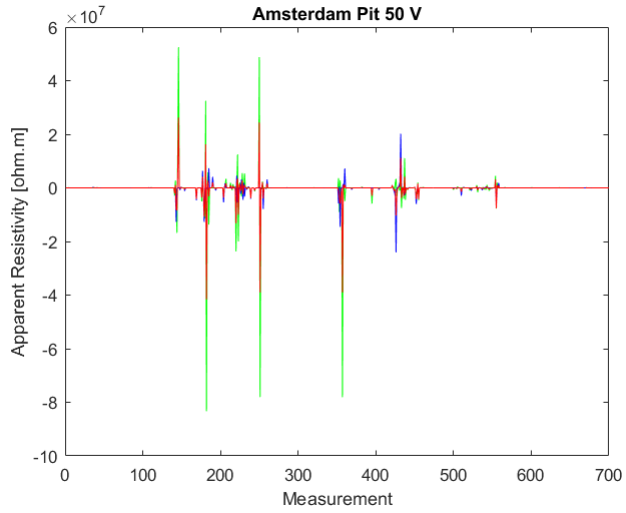

Figure 45: Data empty pit 50V

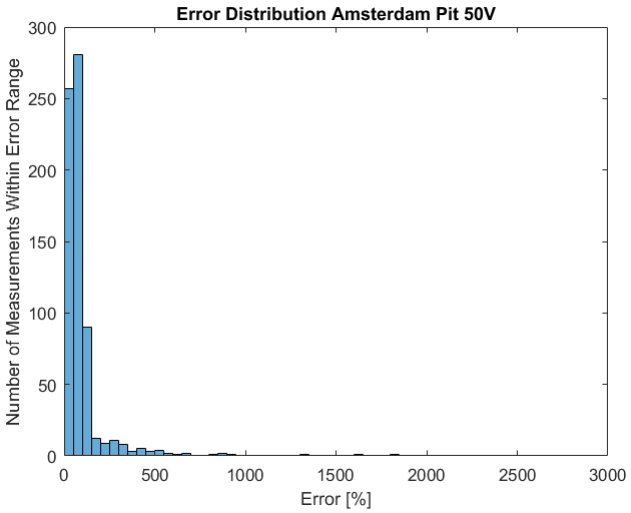

Figure 46: Errors empty pit 50V

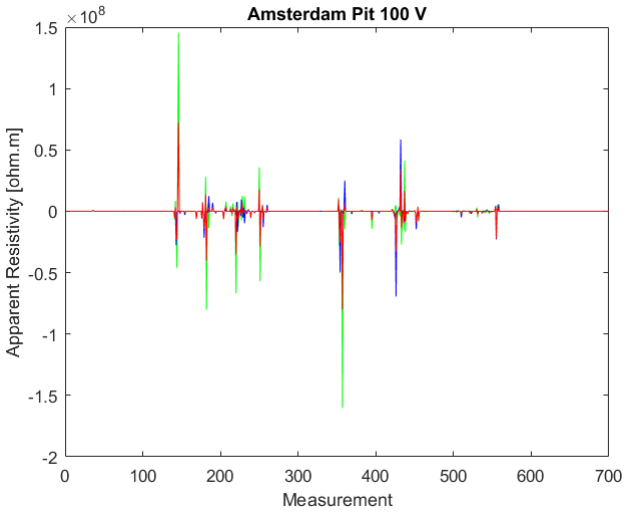

Figure 47: Data empty pit 100V

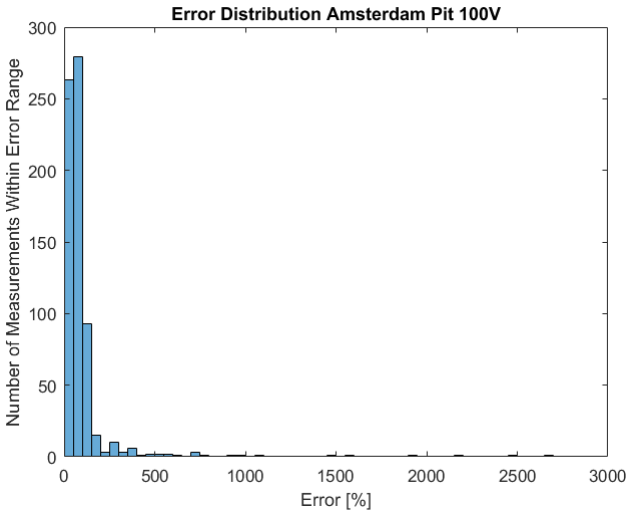

Figure 48: Errors empty pit 100V

A.6 ARISTA Results for the 2D dipole-dipole surveys

Figures 49 through 52 show the resistivity models of the burial site in Amsterdam. They have been 'clipped' to a depth of about 0.5 meters. The bodies have been buried in a pit 0.6 meters deep so at this depth an anomaly could be expected.

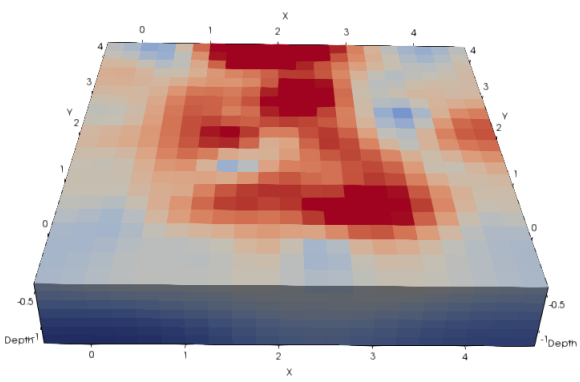

Figure 49: Amsterdam burial 50V normal

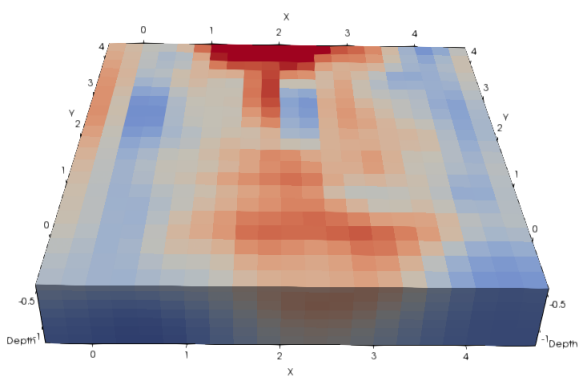

Figure 50: Amsterdam burial 50V reciprocal

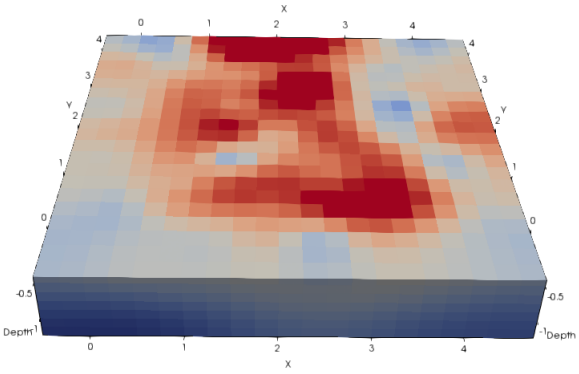

Figure 51: Amsterdam burial 100V normal

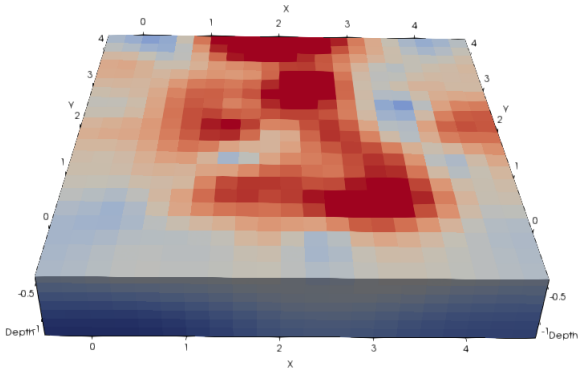

Figure 52: Amsterdam burial 100V reciprocal

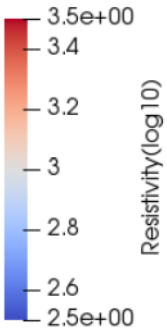

Figure 53: Colour scale used for burial site resistivity models

Due to issues with the IRIS instrument used, which is explained in Section 5, the accuracy of the burial resistivity models is uncertain. When comparing the data sets visually they do seem quite similar, especially the 50V normal compared to the 100V normal/reciprocal. However when comparing them using plots and error calculations shown in the appendix, the magnitude of the errors give rise to uncertainty. Only the normal and reciprocal models for the 100V are comparable, but the range of values in the data is large enough that it is expected that the IRIS was already making faulty measurements at this point.